Zr and Hf oxoclusters as building blocks for the preparation of nanostructured hybrid materials and binary oxides MO_2–SiO_2 (M = Hf, Zr)

Lidia Armelao,[a] Helmut Bertagnolli,[b] Silvia Gross,*[a] Venkata Krishnan,[b] Urska Lavrencic-Stangar,[c] Klaus Müller,[b] Boris Orel,[c] Gokulakrishnan Srinivasan,[b] Eugenio Tondello[d] and Andrea Zattin[d]

Received 7th February 2005, Accepted 3rd March 2005
First published as an Advance Article on the web 12th April 2005
DOI: 10.1039/b501904d

Silica materials embedding ZrO_2 or HfO_2 were prepared by copolymerisation of organically modified oxozirconium or oxohafnium clusters $M_4O_2(OMc)_{12}$ (M = Zr, Hf and OMc = methacrylate) with (methacryloxymethyl)triethoxysilane or (methacryloxypropyl)trimethoxysilane. Free radical copolymerisation of the oxoclusters bearing 12 methacrylate groups with the methacrylate-functionalized siloxanes allows stable anchoring of the clusters to the silica network formed by the hydrolysis and condensation of the alkoxy groups. This route represents a valuable strategy to yield a very homogeneous dispersion of the MO_2 precursors inside the silica matrix. The composition and the microstructural features of the starting hybrid gels were studied by solid state ^{13}C and ^{29}Si NMR spectroscopy and FT IR transmission spectroscopy. Their evolution upon mild heating (up to 180 °C) was followed by FT-IR Attenuated Total Reflectance spectroscopy (ATR), while their thermal behaviour was studied by thermogravimetric analysis (TGA). The covalent incorporation of the clusters into the silica hybrid matrix was studied at several temperatures. Through X-Ray Diffraction (XRD) and Extended X-ray Absorption Fine Structure Spectroscopy (EXAFS) it is demonstrated that temperatures above 800 °C yield binary oxides MO_2–SiO_2 (M = Zr, Hf). Delayed crystallisation of HfO_2 and tetragonal ZrO_2 from 450 °C to at least 800 °C was detected, which is ascribed to the presence of a homogeneous dispersion of the guest oxide in the silica matrix.

1. Introduction

Novel materials endowed with enhanced mechanical, electric, magnetic, electronic and thermal properties can be obtained by combination of inorganic and organic units at the molecular level.[1–5] To ensure the attainment of these properties, an even distribution of the guest building blocks in the host matrix and the absence of grain agglomeration are necessary requirements. The preparation of hybrid inorganic–organic materials using precursors displaying remarkably different chemico-physical properties is a widely investigated issue in materials science.[6] In particular, in nanostructured composites obtained by the incorporation of inorganic building blocks into organic or hybrid inorganic–organic host matrices, relevant factors in determining the desired properties are the homogeneous dispersion of the components and the absence of phase separation. To control the composition of the material, as well as the microstructure and the mutual arrangements of the building blocks, and consequently the features and the performances of the final hybrid system,[7] a route yielding a strong chemical bond among the components is highly desirable. In this framework, several synthetic strategies have been devised which result in a stable anchoring and an even distribution of the guest components in the host matrix. In particular, many efforts have been devoted to the incorporation of host particles in a silica network, which can be conveniently achieved by the sol–gel process.[8] This powerful synthetic method, mainly based on the hydrolysis and condensation of metal alkoxides, provides a reliable route to oxide materials as well as to inorganic–organic hybrid materials.[9,10] To circumvent the drawbacks associated with the formation of inhomogeneities in the composite materials, which are detrimental for many applications, the use of organofunctional silanes of the type $R_nSi(OR')_{4-n}$ ($1 < n < 4$) as coupling agents has gained growing attention.[9] The general OR′ (R′ = Me, Et, Pr *etc.*) alkoxy group undergoes, in the presence of water and of a catalyst, sol–gel hydrolysis and condensation reactions to give the silica network. The organofunctional group R, typically an acrylic or methacrylic moiety, can be chemically bonded to a polymer chain to afford a homogeneous intermixing of the two networks. In a typical approach, based on the use of these organofunctional silanes, cross-linking between an organic polymer (covalently bonded to the R moiety) and the inorganic oxide network (built by sol–gel process of the OR′ groups) can be promoted, leading to the formation of homogeneous materials in which the polymer network is interpenetrated with the silica backbone.[11–13]

To further improve the properties of these materials, the incorporation of other metal alkoxides (Ti, Zr, Hf, Al, *etc.*) has been extensively used.[14] Up to now, such hybrid materials containing different oxide precursors have been prepared by simply mixing metal alkoxides with

*silvia.gross@unipd.it

methacryloxypropyltrimethoxysilane and methacrylic acid as complexing ligands bearing the polymerisable moiety.[11,15] This modified sol–gel procedure, based on the use of different chelating agents to lower the high reactivity of metal alkoxides, has been employed for instance to prepare Si–Ti–Zr based sols.[16]

These hybrid materials, in which metal oxide precursors are homogeneously grafted to a silica matrix, can also be conveniently used for the preparation, upon calcination, of binary oxide systems of the type MO_x–SiO_2, in which the guest metal oxide is evenly dispersed in the silica matrix. In particular, mixed zirconia–silica and hafnia–silica materials are potentially useful for a wide spectrum of technological applications, such as catalysis,[17–20] structural materials and materials with enhanced physico-chemical properties (high thermal and chemical stability or fracture toughness).[21]

The properties of these binary systems are strongly affected by the composition, the microstructure and the degree of mixing of the two oxide components. Consequently, the choice of a suitable synthetic route enabling control of the mentioned characteristics would allow fine tailoring of the properties. These binary systems have been recently prepared by chemical solution deposition[22] and by a conventional sol–gel process starting from the corresponding alkoxides.[23–25] Another study involved the use of the single-source precursor tris(*tert*-butoxy)siloxy complexes $M[OSi(O^tBu)_3]_4$ (M = Zr, Hf) to prepare homogeneous zirconia–silica and hafnia–silica materials.[26] These single-source precursors, however, only result in a binary system characterized by a 1 : 4 MO_2–SiO_2 molar ratio. For many applications, a variation of the MO_2–SiO_2 molar ratio is instead desired, which requires a synthetic route enabling the variation of both SiO_2 and MO_2 precursors.

In the present study, an alternative route to homogeneous mixed oxide materials (MO_2 : SiO_2 (M = Zr, Hf)) by utilizing two methacryloxysilanes as precursors is investigated. This approach relies on the use of the two methacrylate-substituted transition metal oxoclusters of the type $M_4O_2(OMc)_{12}$ and of two different methacryloxysilanes, namely (methacryloxymethyl)triethoxysilane (MAMTES) or (methacryloxypropyl)-trimethoxysilane (MAPTMS). The alkoxy groups of the silane undergo hydrolysis and condensation reactions to give a silica network, while the methacrylate moieties of the cluster and those of the silane are polymerised, giving rise to the incorporation of inorganic building blocks into organic polymers. Such metal oxoclusters have been already used as inorganic building blocks for the synthesis of a wide variety of inorganic–organic hybrid materials.[27–33] The composition and the structure of the composite silica gels embedding the two clusters are investigated. The hybrid sol–gel materials are furthermore used to obtain the corresponding binary oxide systems which should be highly homogeneous on a molecular level. The obtained materials are thoroughly investigated as-prepared, under heating (rt–180 °C) and after calcination at high temperatures by different analytical tools, such as IR, NMR spectroscopy, EXAFS and X-ray diffraction, providing complementary information concerning their composition and microstructure. In particular, ^{13}C and ^{29}Si solid-state NMR spectroscopy is used to characterize the composition of the inorganic–organic hybrid materials and yield information about the degree of polymerisation of the methacrylate groups and condensation of the silica network. XRD and EXAFS are instead employed to study the microstructural features of the final oxides obtained by calcination of the hybrid materials.

2. Experimental

Chemicals

Zirconium(IV) n-butoxide (80% in n-butanol, purchased from Strem Chemical), hafnium(IV) n-butoxide (95% in n-butanol), methacryloxymethyltriethoxysilane and methacryloxypropyl-trimethoxysilane (purchased from Gelest), methacrylic acid 99%, anhydrous tetrahydrofuran and anhydrous toluene (purchased from Aldrich) were used as received and then stored under argon. The polymerisation thermal initiator dibenzoylperoxide was purchased by Aldrich.

Preparation of the starting solution

Due to the high moisture- and air-sensitivity of the precursors, all handlings in the preparation of the solutions were performed under argon using standard Schlenk techniques. The preparation of the samples used for the preparation of the gels is schematically sketched in the flow chart of Fig. 1 and involves three different steps.

First, the methacryloxysilane (MAMTES or MAPTMS) was dissolved in THF and prehydrolysed with water in the presence of HCl as catalyst for 8 h at room temperature. The prehydrolysis conditions have been previously optimised, as reported elsewhere,[34] on the basis of time-resolved ATR and

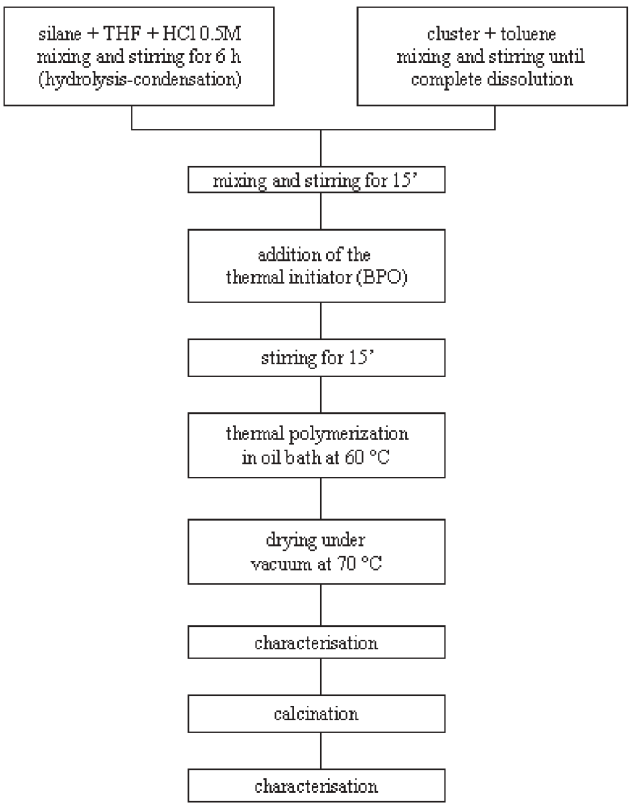

Fig. 1 Flow chart of the synthetic procedure.

NMR data. Typical molar ratios in the sol–gel solution were methacryloxysilane : H_2O : HCl = 1 : 4 : 0.04. The clusters $M_4O_2(OMc)_{12}$ were separately synthesised by following the procedure already described in previous works.[29,35] A weighed amount of the crystalline cluster was dissolved in toluene and this solution was then mixed with the prehydrolysed methacryloxysilane and stirred at room temperature for 15 min. To this solution the initiator dibenzoylperoxide was added (1% w/w with respect to the silane monomer) under stirring. The obtained solutions were heated at 60 °C until polymerisation occurred. A typical polymerisation time was about 1 h. Different samples (see Table 1) were prepared by varying a) the type of cluster (Hf or Zr), b) the type of methacryloxysilane (MAMTES and MAPTMS), c) the methacryloxysilane : cluster molar ratio to investigate how the different parameters affect the final compositional and microstructural features of the system. As references, MAMTES and MAPTMS were also sol–gel processed and thermally cured without the addition of hafnium or zirconium clusters to give the materials labelled as Si-m and Si-p, respectively.

Table 1 summarises the different molar ratios used for the preparation of the samples, according to the nominal composition of the solution. In the Table 1 and in the following, the labels "SiZr" and "SiHf" indicate specimens prepared by using zirconium and hafnium oxoclusters, respectively, the number indicates the Si/M (M = Zr, Hf) atomic ratio, while "m" and "p" indicate the silanes MAMTES (m) and MAPTMS (p), respectively, used for the materials preparation.

After polymerisation, the hafnium and zirconium based gels were dried under vacuum at 70 °C for 12 h to eliminate the residual solvent. A part of the prepared gels was thermally annealed at 800 °C for 3 h in air to promote pyrolysis of the organic components and their conversion to the corresponding binary oxides. Selected samples were further annealed at 1000 °C for 5 h to study their crystallisation behaviour.

Materials characterization

FT-IR absorbance spectra were recorded at room temperature in the transmission mode with a Nexus 870 FT-IR spectrometer (Nicolet) on all the samples before and after thermal calcination. The spectra were recorded in the range 400–4000 cm^{-1}, by averaging 32 scans and using a resolution of 4 cm^{-1}. The solid samples were finely ground and analysed by dispersing them into pellets of spectroscopic grade potassium bromide (purchased from Aldrich).

Table 1 Sample labelling

Sample	Si/M molar ratio
Si-m	—
SiZr37-m	37
SiZr10-m	10
Si-p	—
SiZr43-p	43
SiZr9-p	9
SiZr3-p	3
SiHf17-m	17
SiHf5-m	5
SiHf50-p	50
SiHf15-p	15

Solid-state NMR experiments were carried out on a Bruker MSL 300 spectrometer operating at a static magnetic field of 7.05 T using a 4 mm magic angle spinning (MAS) probe. ^{13}C and ^{29}Si NMR experiments were done at 75.47 MHz and 59.6 MHz, respectively. ^{13}C and ^{29}Si NMR spectra were recorded under MAS conditions (sample rotation frequency: 5 kHz) with cross-polarization (CP) excitation, using $\pi/2$ pulse widths of 4.0 μs. During the CP experiments spin lock fields of 62.5 kHz and contact times of 3 ms were employed at recycle delays of 6 s. Typical numbers of scans were 2048. The ^{29}Si and ^{13}C chemical shifts were determined relative to external standards of Q_8M_8, the trimethylsilylester of octameric silicate, and adamantane, respectively. These values were then expressed relative to TMS (δ = 0 ppm).

The infrared measurements of powder samples at different temperatures (up to 180 °C) were carried out on a Perkin-Elmer System 2000 spectrometer. The attenuated total reflectance (ATR) cell (Golden Gate™ single reflection ATR cell (Specac)) was used equipped with diamond as a ATR crystal. A Golden Gate™ heated diamond ATR top-plate was connected to the temperature controller in order to perform *in-situ* analysis of the powders at different temperatures. The spectra were recorded at various temperatures during heating and cooling of the powders inside a sample compartment that was continuously purged with dry nitrogen.

The thermogravimetric analyses (TGA) were performed in air on a LabSys Setarm SDT 2960 instrument in the temperature range 20–800 °C using a heating rate of 10 °C min^{-1}.

The XRD data were collected with a Bruker D8 Advance Diffractometer equipped with a Göbel mirror. The angular accuracy was 0.001° and the angular resolution was better than 0.01°. The average crystallite sizes were calculated by means of the Scherrer formula from the most intense peaks of each spectrum.

The EXAFS measurements on SiHf5-m and SiHf17-m calcined at 800 °C for 3 h were performed at the Hf L_{III}-edge at 9561 eV with a Si (111) double crystal monochromator, at the XAS beam-line of the Angstroemquelle Karlsruhe (ANKA) at the FZK, Karlsruhe while the measurements on SiZr9-p, calcined at 800 °C for 3 h, was performed at the Zr K-edge at 17998 eV with a Si (311) double crystal monochromator, at the beam-line X1.1 of the Hamburger Synchrotron Radiation Laboratory (HASYLAB) at DESY, Hamburg. Energy calibration was monitored using a 20 μm thick metal foil of the respective element. The data were analysed with a program package especially developed for the requirements of amorphous samples.[36] The AUTOBK[37] program was used for the removal of background and the EXCURV92[38] program was used for evaluation of the EXAFS function. Curved wave theory was used for data analysis in k space and the resulting EXAFS function was weighted with k^3. The mean free path of the scattered electrons was calculated from the imaginary part of the potential (VPI set to −4.00), the amplitude reduction factor AFAC was fixed at 0.8 and an overall energy shift ΔE_0 was introduced to give a best fit to the data.

3. Results and discussion

The as-prepared samples were analysed before and after heat treatment at high temperature to investigate how their structure changed upon heating. Furthermore, their behaviour under heating was also investigated through thermal analysis and temperature-resolved ATR. For the sake of clarity, the data obtained are separately described and discussed.

3.1. As-prepared xerogels

The as-prepared xerogels on the thermally annealed specimens were initially characterised by FT-IR spectroscopy to investigate the variation of chemical composition under heating. In the following, data concerning the as-prepared series of samples are described. As can be seen in the spectrum reported in Fig. 2, already in the crude xerogel embedding zirconium (2a) and hafnium (2b), and based on the MAMTES precursor, typical vibrations of the silica network are present. They will be first discussed, while the bands of the methacrylate groups will be considered next.

In particular, the bands at 1101 cm^{-1} and at 805 cm^{-1} ascribed to the asymmetric ν_{as} and symmetric stretching ν_s of the siloxane group Si–O–Si respectively,[39] were well evident in all the acquired spectra. Furthermore, a third band at 460 cm^{-1} was also detected in the spectrum, which is ascribed to the rocking vibration perpendicular to the Si–O–Si plane.[39]

In the as-prepared samples, bands ascribed to the carboxyl moiety of the methacrylate groups were also detectable. In particular, in all the spectra, the band of the C=O vibration at 1722 cm^{-1} and that at 1320 cm^{-1} of the C–O ester groups were evident. The position of the C=O mode at 1722 cm^{-1} is typical of the C=O mode conjugated with the C=C mode. A shoulder band was expected at 1703 cm^{-1} attributed to the H-bonded C=O mode conjugated with the C=C mode. The presence of this band could be inferred from the poorly discernable shoulder appearing in this range.

Additional bands expected in the spectra of Hf- and Zr-containing samples are the bands of the carbonyl groups of the clusters grafted to the sol–gel matrix. We noticed new bands at 1565 cm^{-1} and 1425 cm^{-1} which we ascribed to the asymmetric and symmetric vibrations of the chelating carboxylate groups.[40] These assignments were corroborated by the increasing intensity of these modes in the spectra of samples containing higher amounts of clusters (Fig. 3), while these two bands were absent in the spectra of pure methacryloxysilanes.

The C=C stretching mode of the methacrylate groups, appearing at 1635 cm^{-1}, is characteristic for all the spectra including those containing different amount of Si/Zr or Si/Hf clusters. In fact, this band should disappear upon complete polymerisation of the methacrylate groups, which, however, does not hold for the samples examined here, as shown by the present IR data as well as by the solid state NMR studies (see below).

The lack of complete polymerisation of the methacryloxy moieties of the silane can probably be ascribed to the hampered mobility of the methacrylate groups, which are covalently linked to the already partially formed silica network. Furthermore, the steric hindrance of the two isostructural clusters, both bearing 12 methacrylate groups, is also expected to play a role in preventing the complete copolymerisation of the cluster itself with methacryloxysilane, thus explaining the presence of unreacted double bonds. The spectra show also the presence of the stretching of the methyl group of the Si–O–CH_3 group at 2840 cm^{-1}. The spectra of the as-prepared samples are moreover characterised by a broad band at 3400 cm^{-1} and by a band at 945 cm^{-1}, ascribed to the Si–OH stretching of the silanols of the not completely condensed silica network.[22] This latter band also occurs in the spectrum of MAPTMS (data not shown) at about 910 cm^{-1}. As will be shown in the section dedicated to calcined samples, the intensity of these bands decreases remarkably upon heating. The described spectral features are common to all the samples characterised by different amounts of zirconium clusters. Similar results were obtained in the case of hafnium-based hybrid materials.

The inorganic–organic hybrid materials based on both types of methacryloxysilanes (see schematic structures in Figs. 4 and 5) were also studied by solid-state ^{13}C and ^{29}Si NMR spectroscopy, which provides useful information on the degree of polymerisation of the methacrylate groups and on the degree of condensation of the silica network. ^{13}C CP/MAS NMR spectra of the hybrids, obtained by polymerisation of

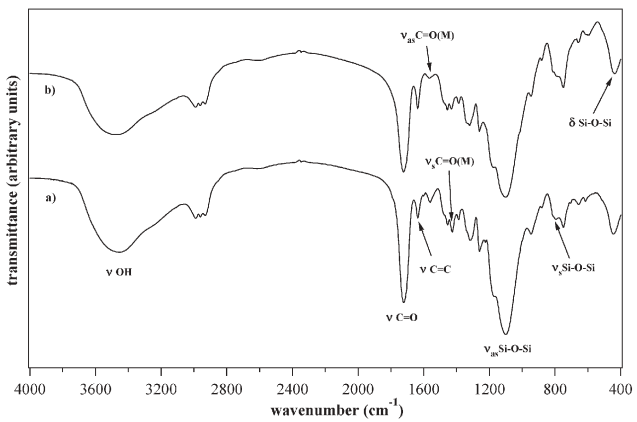

Fig. 2 FT-IR spectra of the as-prepared gels: a) SiHf5-m and b) SiZr10-m.

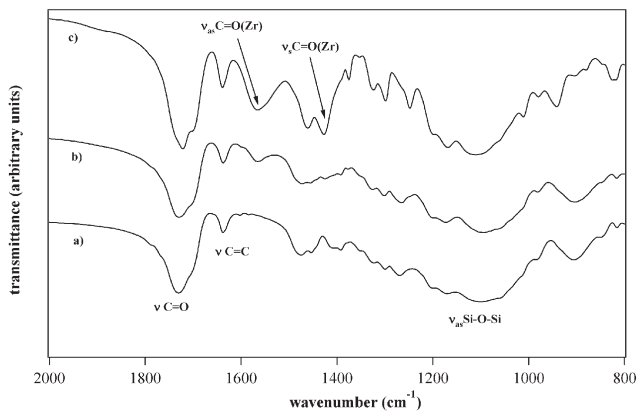

Fig. 3 Comparison of the spectra of the as-prepared: a) Si-p, b) SiZr9-p, c) SiZr3-p

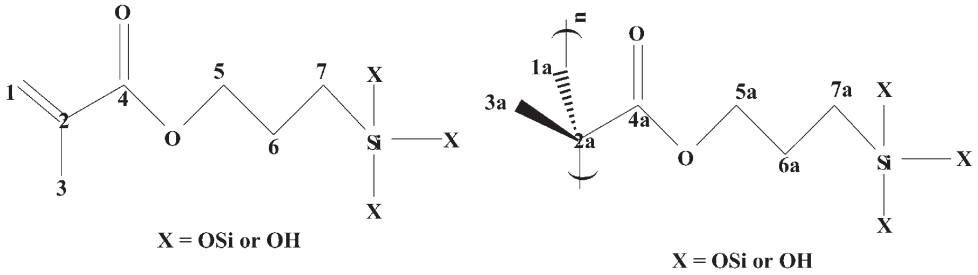

Fig. 4 Chemical structures of hydrolyzed MAPTMS (left), and of the derived polymer (right).

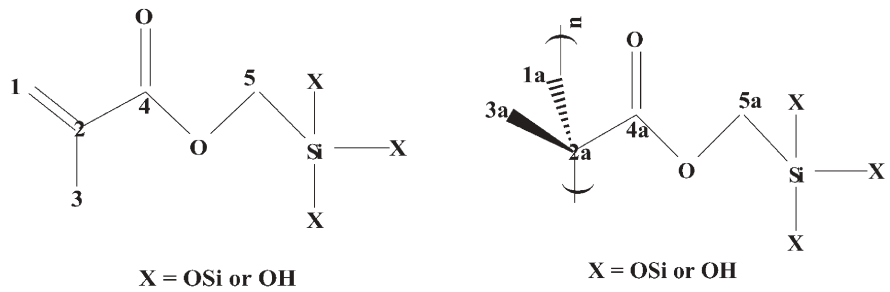

Fig. 5 Chemical structures of hydrolyzed MAMTES (left), and the derived polymer (right).

pre-hydrolysed MAPTMS with zirconium and hafnium oxoclusters in different ratios, are depicted in Fig. 6.

For comparison, the ^{13}C NMR CP/MAS spectrum of the neat polymer, prepared by polymerising pre-hydrolysed MAPTMS, is also given. The peak assignment for these materials (see labels in the upper spectrum of Fig. 6, the chemical structures in Fig. 4 and Tables 2 and 3) was carried out on the basis of the available literature on related compounds.[41–45]

An inspection of the chemical shift values in Tables 2 and 3 reveals that they are very close to the literature values and almost independent of the presence of the cluster in the hybrid materials. In agreement with former studies on polymethylmethacrylate, some variation of the chemical shift was expected for the methyl group (C-3a) of the polymer, reflecting the presence of different isomers.[44] Likewise, the CH_2 group (C-7, C-7a), directly bonded to silicon (signal at $\approx$10 ppm), is characterized by a distribution of chemical shift values which is associated with different environments for the Si atom, as expressed by the T^1, T^2 or T^3 groups (see below).[45]

^{13}C NMR spectroscopy can be used to obtain qualitative information about the degree of polymerisation by investigating the polymerised methacrylate groups, since carbon atoms C-1, C-2, C-4 and C-1a, C-2a, C-4a in the polymeric and non-polymerised materials are clearly distinguished by their chemical shift values. The present ^{13}C NMR data thus clearly prove that the hybrids obtained by copolymerisation of prehydrolysed MAPTMS with the oxoclusters, as well as the specimen without oxoclusters, were not completely polymerised, as also indicated by the aforementioned FT-IR results (see above).

^{13}C CP/MAS NMR spectra were also recorded for two hybrids obtained by copolymerisation of hydrolysed MAMTES with the zirconium oxocluster. The spectra are reported in Fig. 7 along with the reference spectrum of the neat polymer, prepared from hydrolysed MAMTES.

The peak assignment is shown by the labels in the upper spectrum in this figure while the chemical structures are reported in Fig. 5. The experimental chemical shift values, summarised in Tables 4 and 5, are consistent with the literature values for related compounds.[41–45] As found for the former samples based on MAPTMS, the MAMTES samples are also characterised by a finite amount of non-polymerised silanes, as could be deduced from the two sets of signals in the methacrylate group.

The aforementioned inorganic–organic hybrid materials were further characterised by ^{29}Si NMR spectroscopy to investigate the degree of cross-linking of the silica-based network. The corresponding ^{29}Si CP/MAS NMR spectra are depicted in Figs. 8 and 9 for MAPTMS and MAMTES-based materials, respectively.

For the polymer obtained from pre-hydrolysed MAPTMS and the respective copolymers with zirconium and hafnium oxoclusters, the ^{29}Si NMR signals of the tri-functional silanes (T) were located in the range -45 and -70 ppm (see Fig. 8 and Table 6). These values refer to tri-functional groups without cross-linking (T^1) at -48 ppm, with partial (T^2) at -56 ppm, and with complete cross-linking (T^3) in the range -66 to -68 ppm.[46,47] Furthermore, it can be seen that the T^2 units possessed the highest intensity, which holds for all MAPTMS samples. Thus, the degree of cross-linking in the silica network for the present hybrids is very low. The degree of cross-linking was even further reduced if the amount of zirconium and hafnium clusters increased (see Table 7).

It might be speculated whether steric hindrance due to the presence of the oxoclusters is responsible for the less efficient condensation of the silane moieties. A high-field shift of about 10 ppm was registered for the ^{29}Si NMR signals of the hybrid samples based on MAMTES (see Fig. 9), bearing a methylene spacer, when compared to the samples from MAPTMS with a propylene spacer.

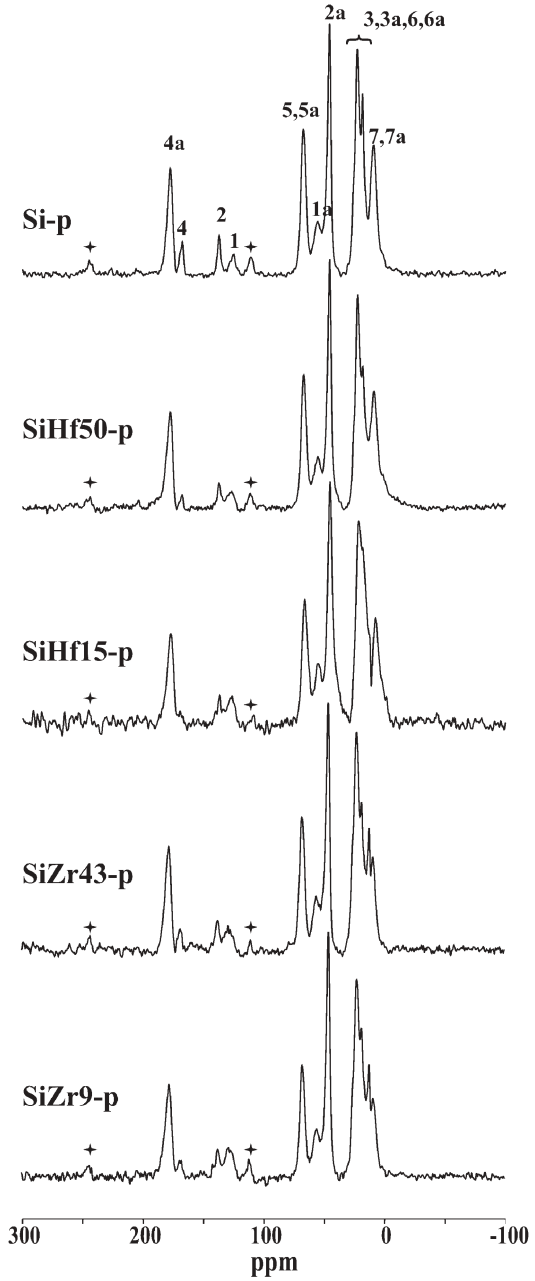

Fig. 6 ^{13}C CP/MAS NMR spectra of polymerized MAPTMS, and copolymers with hafnium and zirconium oxoclusters.

Table 2 ^{13}C chemical shift values of hydrolysed MAPTMS

Carbon no.	Chemical shift (ppm)
1	125.1–127.2 (126)
2	136.8–137.7 (137)
3	18–22.7 (18)
4	167.7–168.7 (167)
5	66.4–67.8 (67)
6	21.7–22.7 (22)
7	7.8–12.2 (9)

This shift is due to the intramolecular activation of the silicon moiety by electron transfer from the ester group *via* the methylene group either through space *via* the sigma bonds, or

Table 3 ^{13}C chemical shift values of polymerized and hydrolysed MAPTMS

Carbon no.	Chemical shift (ppm)
1a	55.2–56.0 (55)
2a	45.4–46.0 (45)
3a	18–22.7 (17.2–21.8)
4a	177.3–178.0 (177)
5a	66.4–67.8 (67)
6a	21.7–22.7 (22)
7a	7.8–12.2 (9)

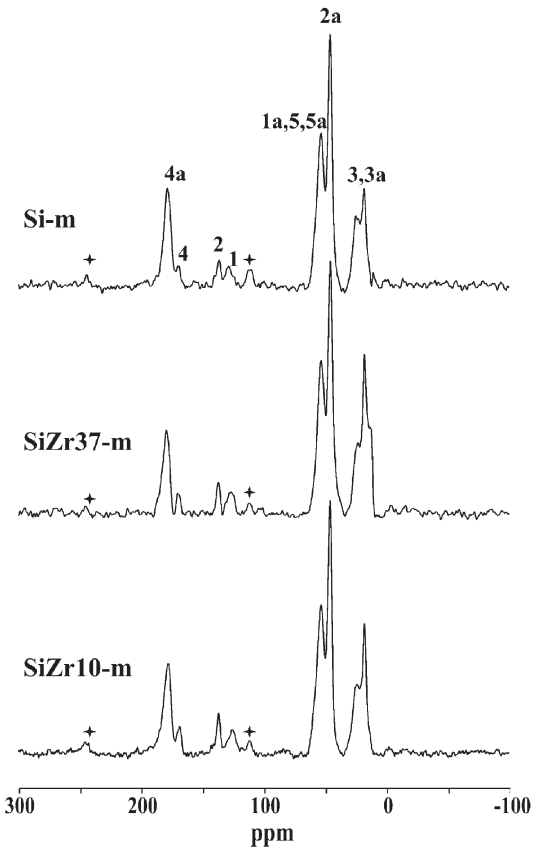

Fig. 7 ^{13}C CP/MAS NMR spectra of polymerized MAMTES, and copolymers with zirconium oxoclusters.

Table 4 ^{13}C chemical shift values of hydrolysed MAMTES

Carbon no.	Chemical shift (ppm)
1	125.9–128.8 (126)
2	136.5–137.1 (137)
3	18–24.3 (18)
4	168.7–170.2 (167)
5	53.4 (58.1)

Table 5 ^{13}C chemical shift values of polymerized and hydrolysed MAMTES

Carbon no.	Chemical shift (ppm)
1a	53.4 (55)
2a	45.9–46.1 (45)
3a	18–24.3 (17.2–21.8)
4a	178–179.5 (177)
5a	53.4 (58.1)

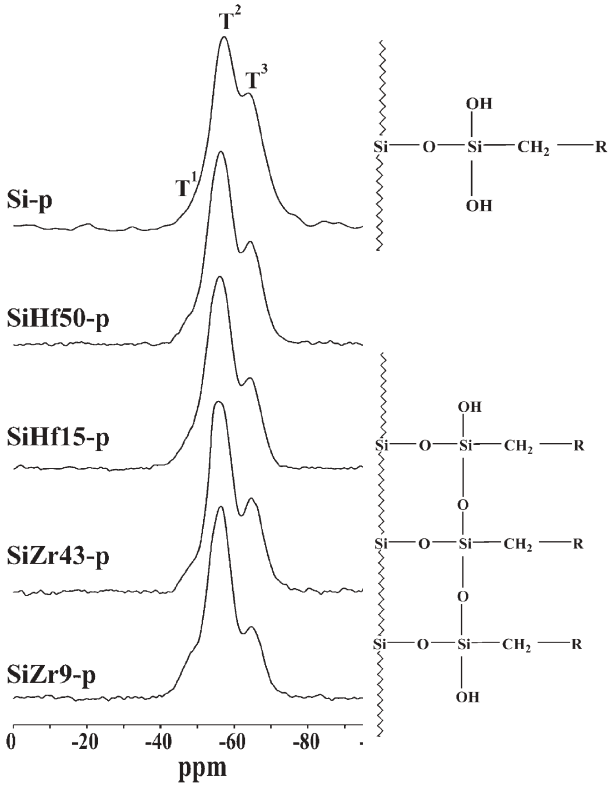

Fig. 8 ^{29}Si CP/MAS NMR spectra of polymerized MAPTMS, and copolymers with hafnium and zirconium oxoclusters.

by hyper-conjugation.[48] The corresponding ^{29}Si NMR signals of the T^1, T^2 and T^3 units were thus found at −57, −66 and −76, respectively.

Again, for the neat polymerised MAMTES, the T^2 signal exhibited the highest relative intensity, indicating a lower degree of cross-linking in the silica network. Incorporation of the zirconium oxocluster was accompanied in this case by a significant alteration of the relative peak intensities. As a result, the largest ^{29}Si NMR signal was found for the T^3 units, reflecting an overall increase of the degree of cross-linking for these doped materials. Such a higher degree of cross-linking can be ascribed to the higher reactivity during the sol–gel process of this latter silane,[48] which is even further enhanced in the presence of the zirconium oxoclusters.

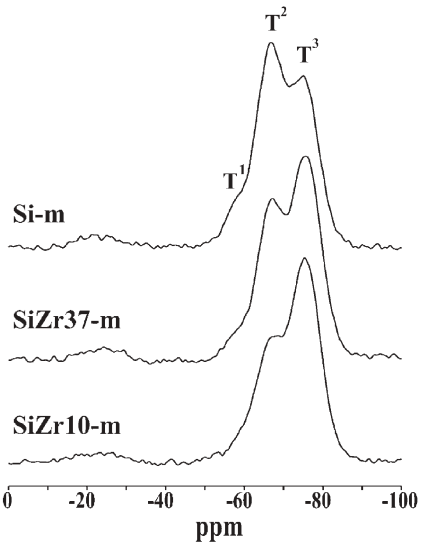

Fig. 9 ^{29}Si CP/MAS NMR spectra of polymerized MAMTES, and copolymers with zirconium oxoclusters.

Table 6 ^{29}Si chemical shift values of the organic–inorganic hybrid materials

Sample	^{29}Si NMR chemical shifts (ppm)		
	T^1	T^2	T^3
Si-p	−50.0	−56.7	−64.9
SiHf50-p	−48.7	−56.4	−65.2
SiHf15-p	−49.9	−56.3	−64.9
SiZr43-p	−47.9	−56.1	−65.2
SiZr9-p	−48.2	−56.2	−65.5
Si-m	−57.0	−66.8	−75.8
SiZr37-m	−57.3	−66.8	−76.0
SiZr10-m	−55.9	−66.5	−75.8

Table 7 Signal intensities from ^{29}Si NMR spectra of organic–inorganic hybrid materials

Sample	Relative signal intensities		
	T^1	T^2	T^3
Si-p	3.5	100	64.5
SiHf50-p	2.6	100	32.5
SiHf15-p	10.1	100	28.3
SiZr43-p	6.8	100	52.7
SiZr9-p	5.7	100	18.9
Si-m	5.6	100	62.8
SiZr37-m	1.8	76.6	100
SiZr10-m	0.1	69.4	100

3.2. Behaviour on heating

The behaviour of the gels on heating was firstly investigated by TGA. Different samples, characterized by different amount of zirconium or hafnium embedded clusters, were analysed in air in the thermal range rt–1000 °C. Undoped Si-m and Si-p were also analysed as references. Comparison of the different thermograms showed that the introduction of the cluster into the siloxane matrix did not sensibly alter the thermal profile of the material. No remarkable shift in the onset of decomposition was observed. This, as indicated by solid-state NMR and IR spectral data, was ascribed to the reduced capability of the cluster to induce cross-linking of the network, stemming from the hampered mobility of the already partially condensed and polymerised inorganic siloxane network.

Previous studies performed on PMMA or polystyrene matrices embedding the same zirconium cluster used in this study[29–31] have shown that the incorporation of the cluster remarkably improves the thermal stability of the hybrid material with respect to the neat polymer. Furthermore, it has been pointed out that the increase of the decomposition onset temperature can be related to the amount of embedded cluster, *i.e.* the higher the amount of cluster, the higher the temperature increase. This finding has been traced back to the enhanced degree of cross-linking determined by the twelve methacrylate groups on the surface of the cluster.

In the present case, as mentioned, no improvement was found, which can be ascribed to the low degree of cross-linking of the material.

For our aims, these findings are not particularly relevant, since the declared aim of the chosen route was to ensure a stable grafting of the cluster to the sol–gel matrix, and to achieve, upon calcination, a homogeneous dispersion of zirconia and hafnia inside the silica network.

The thermal decomposition of the materials occurred in the temperature range 270–580 °C and after 650 °C no further weight loss was detected. The samples embedding the hafnium cluster showed very similar behaviour: also in this case, the embedding of the cluster does not significantly improve the thermal stability.

To investigate evolution towards the final product, ATR infrared experiments were carried out on heating the samples up to 180 °C. First, the ATR spectra (recorded at room temperature) of three xerogel samples containing different amounts of the cluster (Fig. 10: Si-m, SiZr37-m and SiZr10-m) are compared. Si-m is the sample containing no Zr clusters, while the other two were prepared by following the same experimental route but with addition of Zr clusters in the Si/Zr molar ratios of 10 and 37, respectively. All spectra showed the two most intense bands at 1710 cm^{-1}, corresponding to a carbonyl conjugated with C=C, and at 1070–1080 cm^{-1}, which is ascribed to the Si–O–Si stretching modes. The Si–O–Si band is slightly influenced by the incorporation of the cluster and a shift from 1070 cm^{-1} (without clusters) to 1080 cm^{-1} (with larger amount of clusters) was detected. In the sample SiZr10-m with a larger amount of clusters, the bands due to the cluster itself (611 cm^{-1}, 652 cm^{-1}, 1424 cm^{-1} and 1558 cm^{-1}) can be also observed. The bands of cluster carbonyls (ν_{as}C=O at 1556 cm^{-1} and ν_{s}C=O at 1424 cm^{-1}) were shifted with respect to their positions in the spectrum of the pure cluster itself (ν_{as}C=O at 1569 cm^{-1} and ν_{s}C=O at 1413 cm^{-1}), which is a consequence of its dispersion in the silica matrix.

The sample characterised by the higher loading of zirconium cluster (SiZr10-m) was heated inside the sample compartment up to 180 °C. Spectra were recorded *in-situ* at room temperature, 100, 120, 140, 160 and 180 °C (Fig. 11).

The most noticeable effect of heating to 180 °C was the gradual shift of the carbonyl band from its initial position at 1711 cm^{-1} to 1724 cm^{-1} at 180 °C. This is usually ascribed to the change of C=O interactions with its surroundings, *i.e.* from H-bonded carbonyls at lower wavenumbers to more free and non H-bonded carbonyls at higher wavenumbers. Regarding the Si–O–Si vibration around 1080 cm^{-1}, there was no change in the position of this band upon heating, but only an increase in intensity was observed. At the same time the band at ~3400 cm^{-1} (νOH) became less intense already at 100 °C, indicating a densification of the matrix during heating from room temperature to 100 °C. This is in agreement with the curing temperature due to the cross-linker used in this study (70 °C).

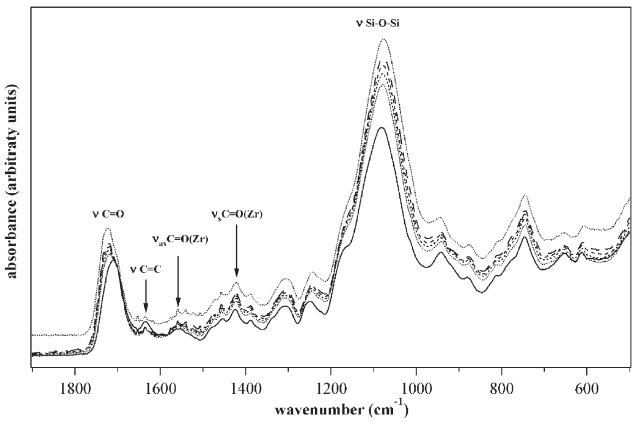

Fig. 11 ATR as a function of increasing temperature of the sample (solid line: initial, dashed line: 180 °C) SiZr10-m.

3.3. Calcined samples: HfO_2–SiO_2 and ZrO_2–SiO_2

IR measurements were also carried out on the calcined samples (Fig. 12). Common features were found in all the samples notwithstanding their composition.

In the annealed samples, the disappearance of all the bands ascribed to the organic part was detected. The intensity and the sharpness of the typical bands of silica increased upon calcination, as expected. In the calcined sample, the only bands detected were those typical of the silica network at 1084, 802 and 460 cm^{-1}, while all the vibrations of organic groups disappeared as a consequence of their pyrolytic combustion. Also the band at 3400 cm^{-1} is remarkably less intense than in

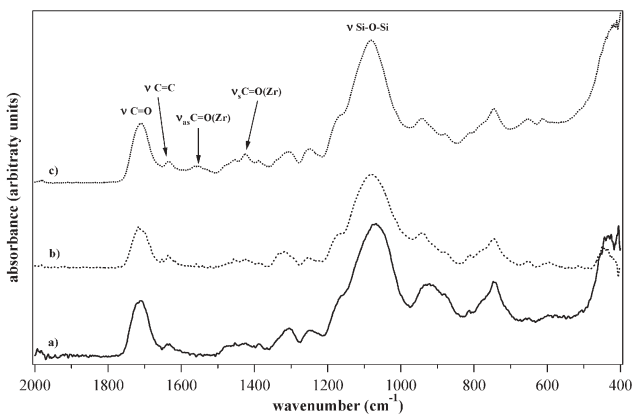

Fig. 10 ATR spectra of a) Si-m, b) SiZr37-m, c) SiZr10-m.

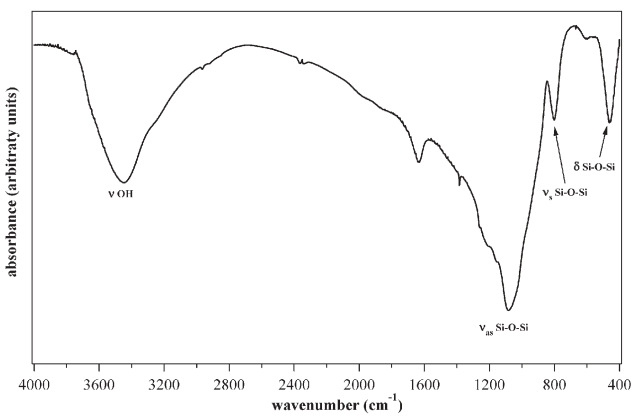

Fig. 12 FT-IR of the gel SiZr10-m calcined for 3 h at 800 °C.

the as-prepared samples, but still present. This finding can be ascribed to a competitive contribution to the formation of new hydroxyl groups upon introduction of ZrO_2 and HfO_2. As reported by Neumayer and Cartier,[22] the increase of hydroxyl content can be ascribed to the disruption of the silica network by ZrO_2 and HfO_2 doping, which results in an increase of terminal non-bridging groups and the consequent adsorption of water from the ambient. Accordingly, also a band ascribed to adsorbed water at about 1635 cm^{-1} was detected.

Also in the calcined samples, no mixed Hf–O–Si or Zr–O–Si bonds were detected. Since the XRD diffractograms (see below) clearly show the formation of crystalline ZrO_2 and HfO_2, this fact can be attributed to the formation of well-defined oxide clusters of small size instead of a continuous mixed network. The chosen approach, relying on the anchoring of the guest particles to a host silica network, would in fact favour the nucleation of small oxide clusters, while their growth is limited by the surrounding silica backbone, to which they are rigidly grafted.

The local structure of the calcined samples was investigated by EXAFS, which is a useful method for probing the neighbourhood environment of a selected atom. The X-ray absorption near edge structure (XANES) region provides information about the coordination geometry and oxidation states of the absorbing atom, while extended X-ray absorption fine structure (EXAFS) spectroscopy provides information about the coordination number, the nature of the scattering atoms surrounding the absorbing atom and the interatomic distance between the absorbing atom and the backscattering atoms.[49]

The experimentally determined and theoretically calculated EXAFS functions of SiHf5-m and SiHf17-m calcined for 3 h at 800 °C are shown in k space, as well as by Fourier transforms in real space, in Figs. 13 and 14, respectively, while the corresponding structural parameters are summarized in Table 8.

In the fitting procedure, the various parameters *i.e.* coordination number, interatomic distance, Debye–Waller factor and energy zero value were determined by iterations. In the analysis of the experimental k^3 weighted $\chi(k)$ function, a three-shell model can be fitted for both SiHf5-m and SiHf17-m. The first shell of SiHf5-m consists of about 2.5 oxygen backscatterers at a distance of about 2.01 Å, whereas SiHf17-m consists of about 4.4 oxygen backscatterers at nearly the same distance. The second shell comprising about 2.5 oxygen backscatterers was found at a distance of 2.15 Å in the case of SiHf5-m, but at distance of 2.22 Å in the case of SiHf17-m. In both samples, the third shell has about 2.4 hafnium backscatterers but at different distances, 3.41 Å in SiHf5-m and 3.47 Å in SiHf17-m. These differences in the structural parameters of SiHf5-m and SiHf17-m could be attributed to the different silane : Hf compositions of the samples. It was not possible to match the structural parameters determined by EXAFS with any of the well-known

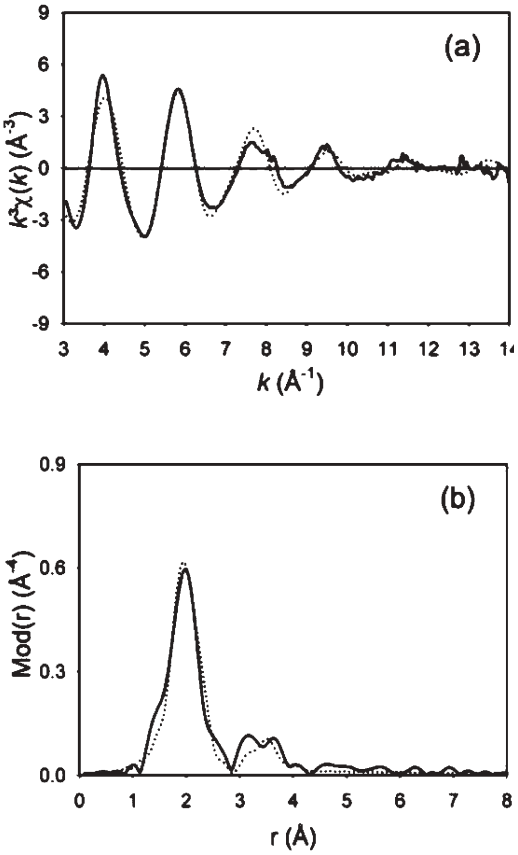

Fig. 13 Experimental (solid line) and calculated (dotted line) EXAFS functions and their corresponding Fourier transforms of SiHf5-m.

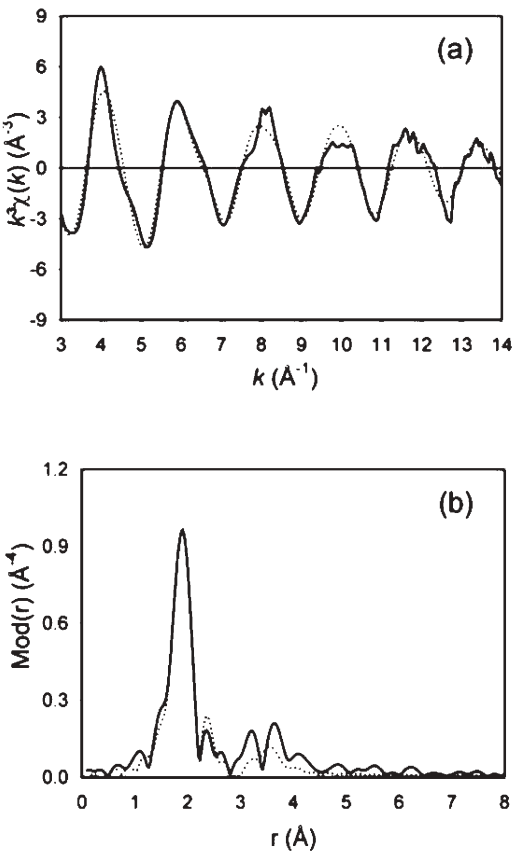

Fig. 14 Experimental (solid line) and calculated (dotted line) EXAFS functions and their corresponding Fourier transforms of SiHf17-m.

Table 8 Structural parameters of the calcined samples SiHf5-m and SiHf17-m determined by EXAFS

Sample	A–Bs[a]	N^b	r^c/Å	σ^d/Å	$\Delta E_0{}^e$/eV	k-range/Å^{-1}	Fit index
SiHf5-m calcined	Hf–O	2.5 ± 0.2	2.01 ± 0.02	0.071 ± 0.007	13.94	3.0–14.0	28.49
	Hf–O	2.6 ± 0.3	2.15 ± 0.02	0.077 ± 0.009			
	Hf–Hf	2.2 ± 0.3	3.41 ± 0.04	0.122 ± 0.016			
SiHf17-m calcined	Hf–O	4.4 ± 0.4	2.00 ± 0.02	0.071 ± 0.007	12.85	3.0–14.0	25.64
	Hf–O	2.4 ± 0.2	2.22 ± 0.02	0.077 ± 0.009			
	Hf–Hf	2.5 ± 0.3	3.47 ± 0.04	0.122 ± 0.016			

[a] Absorber (A)–backscatters (Bs). [b] Coordination number N. [c] Interatomic distance r. [d] Debye–Waller factor σ with its calculated deviation. [e] Shift of the threshold energy ΔE_0.

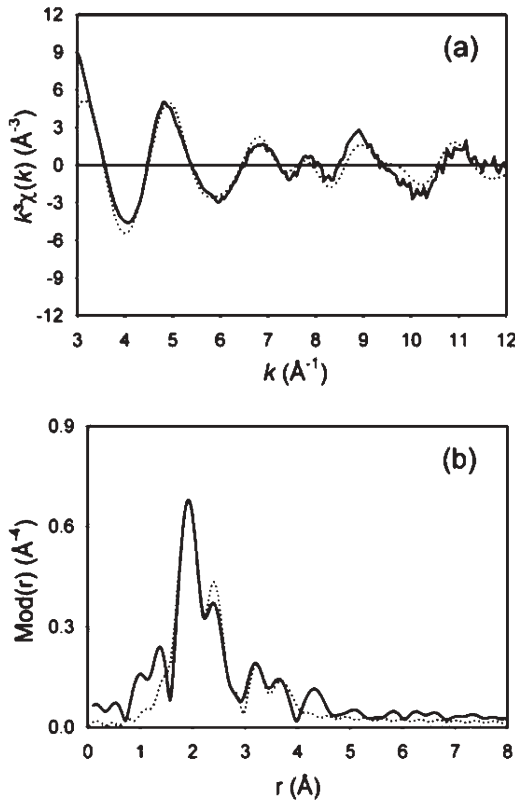

Fig. 15 Experimental (solid line) and calculated (dotted line) EXAFS functions and their corresponding Fourier transforms of SiZr9-p.

polymorphs of crystalline HfO_2. Further, in both the samples distances corresponding to Hf–O–Si mixed bonds could not be evidenced, in agreement with the IR data.

The experimentally determined and calculated EXAFS functions of SiZr9-p are shown in k space, as well as by Fourier transforms in real space, in Fig. 15 and the structural parameters are summarised in Table 9.

In the analysis of the EXAFS function, a three-shell model comprising two oxygen shells and one zirconium shell could be fitted for SiZr9-p. The first shell at a distance of 2.04 Å with about 3.1 backscatterers, the second shell at a distance of 2.24 Å with about 5.5 backscatterers and the third shell at a distance of 3.37 Å with about 1.5 backscatterers were determined. Distances corresponding to Zr–O–Si mixed bonds could not be found, as also indicated by the IR data. The EXAFS determined structural parameters could not be matched with any of the well-known polymorphs of crystalline ZrO_2. In this regard, further information was obtained from the XANES spectra. The comparison of the XANES region of SiZr9-p with those of the tetragonal and monoclinic modifications of ZrO_2 is shown in Fig. 16. It could be observed that the XANES spectrum of SiZr9-p is similar to that of the tetragonal polymorph, characterized by the presence of a twin peak over the absorption edge (see Fig. 16).

Based on this evidence, the formation of tetragonal zirconia already in the sample annealed at 800 °C could be established. The information provided by EXAFS was further integrated and strengthened by XRD.

The crystallisation behaviour of the HfO_2–SiO_2 and ZrO_2–SiO_2 systems has been the topic of several structural studies since phase transitions and changes can strongly affect the properties of the final materials.[22,50–55]

The investigated sample SiZr3-p, characterised by a high loading of zirconia, was heated to 800 °C for 3 h, but after this annealing only a broad peak at 22° typical of amorphous silica was detected. As can be seen in Fig. 17, only after a further annealing at 1000 °C for 5 h was the formation of tetragonal zirconia observed, in agreement with Moon *et al.*[56]

Similar results were achieved in the case of hafnia-containing samples. Also in this case, annealing at 800 °C does not result in crystallisation, while after a further annealing at 1000 °C for 5 h crystallisation of tetragonal hafnia was found (see Fig. 17)

From the diffractograms acquired, the presence of monoclinic zirconia as well as the formation of zirconium silicate could be excluded.

From the Scherrer equation, which allows estimation of the mean crystallite radius from the width of the most intense

Table 9 Structural parameters of the calcined sample SiZr9-p determined by EXAFS

Sample	A–Bs[a]	N^b	r^c/Å	σ^d/Å	$\Delta E_0{}^e$/eV	k-range/Å^{-1}	Fit index
SiZr9-p calcined	Zr–O	3.1 ± 0.3	2.04 ± 0.02	0.071 ± 0.007	17.19	3.0–12.0	35.45
	Zr–O	5.5 ± 0.6	2.24 ± 0.02	0.105 ± 0.011			
	Zr–Zr	1.5 ± 0.2	3.37 ± 0.04	0.107 ± 0.014			

[a] Absorber (A)–backscatters (Bs). [b] Coordination number N. [c] Interatomic distance r. [d] Debye–Waller factor σ with its calculated deviation. [e] Shift of the threshold energy ΔE_0.

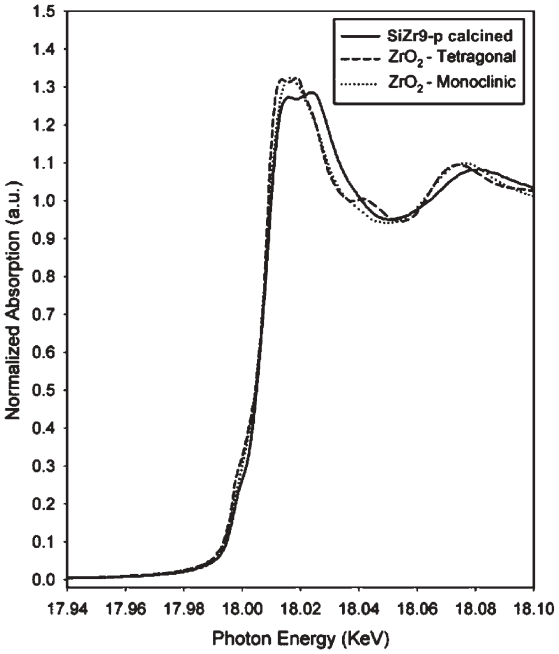

Fig. 16 XANES region of SiZr9-p and the reference ZrO_2 polymorphs.

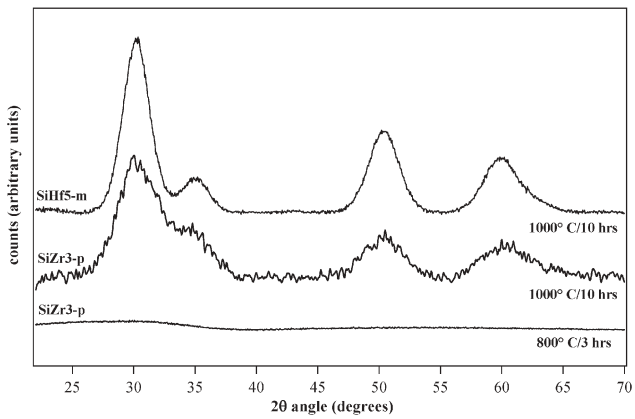

Fig. 17 XRD patterns of the samples SiZr3-p (calcined at 800 °C for 3 h and at 1000 °C 10 h) and of the sample SiHf5-m calcined at 1000 °C for 10 h.

diffraction peak, the average crystallite size was estimated to be about 4 nm.[57,58]

It is well known that zirconia exists in different modifications, namely monoclinic (stable up to 1000 °C), tetragonal, (stable above 1000 °C) and cubic (>2300 °C).[59] Under normal conditions, the thermodynamically stable phase up to 1000 °C is the monoclinic one. A metastable tetragonal phase may be present in pure zirconium dioxide when non-equilibrium techniques of synthesis,[60] leading to high surface area material, are applied. Under these conditions, differences in the specific surface energies of the monoclinic and tetragonal forms may play a remarkable role in the stability criteria.[51] Furthermore, addition of SiO_2 to zirconia or hafnia has been proven to increase the crystallisation temperature of tetragonal zirconia remarkably and also to increase the temperature at which the transformation from tetragonal to monoclinic zirconia takes place.[22] In a previously reported study on the crystallisation of ZrO_2–SiO_2 as a function of ZrO_2 content, crystallisation of tetragonal zirconia was observed at 1000 °C for a sample containing 30% of zirconium. In a similar way, silica stabilises the formation of tetragonal hafnia. According to Terry *et al.*,[26] the initial formation of tetragonal zirconia instead of the thermodynamically expected monoclinic form has also been ascribed not only to surface and strain energies, but also to a hindered tetragonal to monoclinic transformation which, being slightly displacing (3–5% by volume), can be inhibited whenever zirconia is mixed with silica. As a consequence, this increase in the crystallisation temperature in turn has been traced back to the homogeneous distribution of zirconia or hafnia in the silica network. The crystallisation of zirconia would require diffusion and grain growth, which is more difficult whenever zirconia is mixed with silicon dioxide. The existence of this correlation seems to be proved by a decrease in the rate of grain growth for tetragonal zirconia with a decreasing ZrO_2 concentration, as reported by Shoyama *et al.*[61] Based on these results, a homogeneous dispersion of zirconia or hafnia clusters in the silica can be hypothesised.

4. Conclusion

The developed experimental strategy, involving the use of methacryloxy-functionalised silanes, Hf and Zr oxoclusters and a sol–gel/polymerisation two-step process, has been demonstrated to be well suited for preparation of homogeneous multicomponent gels which, upon calcination, evolve to give the corresponding binary oxides, *i.e.* HfO_2–SiO_2 and ZrO_2–SiO_2.

The chosen approach yields materials in which the guest clusters are homogeneously dispersed and in which the clusters are covalently anchored to the silica matrix. The thermolytic conversion of inorganic–organic hybrids represents a novel and advantageous route to retain the homogeneity of the starting xerogels in the final oxide mixed materials.

The materials were investigated as-prepared, under heating and upon calcination. Solid-state NMR and IR data indicated that the incorporation of the cluster does not remarkably modify the structure of the gels, and a low degree of cross-linking in the silica network was observed. Accordingly, no noticeable improvement of the thermal stability of the hybrid materials with respect to the undoped gels was evidenced by thermogravimetric analysis. Evolution under heating was studied by ATR which indicates a progressive densification of the matrix upon annealing and the dispersion of the cluster in the silica matrix.

After calcination, mixed oxides were obtained, whose crystallisation behaviour was studied by EXAFS and XRD. In agreement with the IR data, EXAFS did not demonstrate the formation of Si–O–M bonds, which would be instead observed in case of a binary "solid solution" of zirconia or hafnia in the silica network. At 800 °C no formation of crystalline oxides could be identified by EXAFS, but the XANES spectrum of the zirconium containing sample was similar to that of tetragonal zirconia, which actually forms after annealing at 1000 °C, as shown by the XRD patterns.

Acknowledgements

The National Research Council (CNR), Italy and the Deutsche Forschungsgemeinschaft (DFG), Germany are acknowledged for financial support. The Italian Rector s′ Conference (CRUI) and Deutsche Akademische Austauschdienst (DAAD) are gratefully acknowledged for funding of the researchers mobility in the framework of a Vigoni Programme. We thank ANKA at FZK, Karlsruhe and HASYLAB at DESY, Hamburg for the provision of synchrotron radiation for XAFS measurements. S. Gross thanks CNR for a 2004 Short Term Mobility grant. The authors also thank Roberta Saini and Giuseppe Pace for TGA measurements.

Lidia Armelao,[a] Helmut Bertagnolli,[b] Silvia Gross,*[a] Venkata Krishnan,[b] Urska Lavrencic-Stangar,[c] Klaus Müller,[b] Boris Orel,[c] Gokulakrishnan Srinivasan,[b] Eugenio Tondello[d] and Andrea Zattin[d]

[a]*CNR–ISTM, University of Padova, via Marzolo, 1- I-35131 Padova, Italy. E-mail: silvia.gross@unipd.it*

[b]*Institute of Physical Chemistry, University of Stuttgart, Pfaffenwaldring 55, D-70569 Stuttgart, Germany*

[c]*National Institute of Chemistry, Hajdrihova 19, SI-1000 Ljubljana, Slovenia*

[d]*Department of Chemistry, University of Padova, via Marzolo, 1-35131 Padova, Italy*

References

1 C. Sanchez, F. Ribot and B. Lebeau, *J. Mater. Chem.*, 1999, **9**, 35.
2 C. Sanchez and F. Ribot, *J. Phys.*, 1993, **3**, 1349.
3 J. Wen and G. L. Wilkes, *Chem. Mater.*, 1996, **8**, 1667.
4 K. G. Sharp, *Adv. Mater.*, 1998, **10**, 1243.
5 D. A. Loy, *MRS Bull.*, 2001, 364.
6 L. Spanhel, M. Popall and G. Müller, *Proc. Indian Acad. Sci.: Chem. Sci.*, 1995, **107**, 637.
7 U. Schubert and N. Hüsing, *Synthesis of Inorganic Materials*, Wiley VHC Verlag, Weinheim, 2000.
8 C. J. Brinker and G. W. Scherer, *Sol–Gel Science: The Physics and Chemistry of Sol–Gel Processing*, Academic Press Inc., San Diego, 1990.
9 C. Sanchez and M. In, *J. Non-Cryst. Solids*, 1992, **147–148**, 1.
10 C. Sanchez, M. In, P. Toledano and G. Griesmar, *Mater. Res. Soc. Symp. Proc.*, 1992, **271**, 669.
11 O. Soppera, C. Croutxé-Barghorn, C. Carrè and D. Blanc, *Appl. Surf. Sci.*, 2002, **186**, 91.
12 J. Jang and H. Park, *J. Appl. Polym. Sci.*, 2002, **10**, 2074.
13 H. Jo and F. D. Blum, *Chem. Mater.*, 1999, **10**, 2548.
14 R. Nass and H. Schmidt, *SPIE Sol–Gel Opt.*, 1990, **1328**, 258.
15 O. K. Park, J. I. Jung and B. S. Bae, *J. Mater. Res.*, 2001, **16**, 2143.
16 J. Mendez-Vivar, R. Mendoza-Serna and L. Valdez-Castro, *J. Non-Cryst. Solids*, 2001, **288**, 200.
17 M. Itoh, H. Hattori and K. J. Tanabe, *J. Catal.*, 1974, **35**, 225.
18 J. B. Miller and E. I. Ko, *J. Catal.*, 1996, **159**, 58.
19 H. J. M. Bosman, E. C. Kruissink, J. Vanderspoel and F. Vandenbrink, *J. Catal.*, 1994, **148**, 660.
20 Z. Feng, W. S. Postula, C. Erkey, C. V. Philip, A. Akgerman and R. G. Anthony, *J. Catal.*, 1994, **148**, 660.
21 R. G. Simhan, *J. Non-Cryst. Solids*, 1983, **54**, 335.
22 D. A. Neumayer and E. Cartier, *J. Appl. Phys.*, 2001, **90**, 1801.
23 G. Mountjoy, M. A. Holland, P. Gunawidjaja, G. W. Wallidge, D. M. Pickup, R. J. Newport and M. E. Smith, *J. Sol-Gel Sci. Technol.*, 2003, **26**, 161 and references therein.
24 Z. Zhan and H. C. Zeng, *J. Non-Cryst. Solids*, 1999, **243**, 26 and references therein.
25 J. B. Miller and E. I. Ko, *Catal. Today*, 1997, **35**, 269.
26 K. W. Terry, C. G. Lugmair and T. D. Tilley, *J. Am. Chem. Soc.*, 1997, **119**, 9745.
27 G. Kickelbick, *Prog. Polym. Sci.*, 2003, **28**, 83.
28 U. Schubert, *Chem. Mater.*, 2001, **13**, 3487 and references therein.
29 G. Trimmel, S. Gross, G. Kickelbick and U. Schubert, *Appl. Organomet. Chem.*, 2001, **15**, 410.
30 U. Schubert, G. Trimmel, B. Moraru, W. Tesch, P. Fratzl, S. Gross, G. Kickebilck and N. Hüsing, *Mater. Res. Soc. Symp. Proc.*, 2001, **238**, C.C. 2.3.1.
31 G. Trimmel, B. Moraru, S. Gross, V. Di Noto and U. Schubert, *Macromol. Symp.*, 2001, **175**, 357.
32 S. Gross, G. Trimmel, U. Schubert and V. Di Noto, *Polym. Adv. Technol.*, 2002, **13**, 254.
33 S. Gross, V. Di Noto, G. Kickelbick and U. Schubert, *Mater. Res. Soc. Symp. Proc.*, 2002, **726**, Q4.1.1.
34 S. Gross, A. Zattin, B. Orel, U. Lavrencic-Stangar, A. Sassi and L. Armelao, in preparation.
35 S. Gross, G. Kickelbick, M. Puchberger and U. Schubert, *Monatsh. Chem.*, 2003, **134**, 1053.
36 T. S. Ertel, H. Bertagnolli, S. Hückmann, U. Kolb and D. Peter, *Appl. Spectrosc.*, 1992, **46**, 690.
37 M. Newville, P. Livins, Y. Yakoby, J. J. Rehr and E. A. Stern, *Phys. Rev. B*, 1993, **47**, 14126.
38 S. J. Gurman, N. Binstead and I. Ross, *J. Phys. C*, 1986, **19**, 1845.
39 P. Innocenzi, *J. Non-Cryst. Solids*, 2003, **316**, 309.
40 K. Saravanamuttu, D. Xin Min, S. I. Najafi and M. P. Andrews, *Can. J. Chem.*, 1998, **76**, 1717.
41 L. N. Lewis, T. A. Early, M. Larsen, E. A. Willaims and J. C. Grande, *Chem. Mater.*, 1995, **7**, 1369.
42 P. Innocenzi, G. Brusatin, S. Licoccia, M. L. Di Vona, F. Babonneau and B. Alonso, *Chem. Mater.*, 2003, **15**, 4790.
43 J. Schraml, N. D. Chuy, P. Novak, V. Chvalovsky, M. Mägi and E. Lippman, *Collect. Czech. Chem. Commun.*, 1978, **43**, 3202.
44 Q. T. Pham, R. Petiand and H. Waton, *Proton and Carbon NMR Spectra of Polymers*, Penton Press Ltd, London, 1991, p. 50.
45 A. Jimenez-Morales, P. Aranda and J. C. Galvan, *J. Mater. Proc. Technol.*, 2003, **143–144**, 5.
46 J. Roychen, S. Zhang and W. T. Ford, *Macromolecules*, 1996, **29**, 1305.
47 M. Pursch, L. C. Sander and K. Albert, *Anal. Chem.*, 1996, **68**, 4107.
48 S. Altmann and J. Pfeiffer, *Monatsh. Chem.*, 2003, **134**, 1081.
49 H. Bertagnolli and T. S. Ertel, *Angew. Chem., Int. Ed. Engl.*, 1994, **33**, 45.
50 M. I. Osendi, J. S. Moya, C. J. Serna and J. Soria, *J. Am. Ceram. Soc.*, 1985, **68**, 135.
51 R. C. Garvie, *J. Phys. Chem.*, 1965, **69**, 1238.
52 R. C. Garvie, *J. Phys. Chem.*, 1978, **82**, 218.
53 V. S. Nagarajan and K. J. Rao, *J. Mater. Sci.*, 1989, **24**, 2140.
54 A. H. Heuer, N. Claussen, W. M. Kriven and M. Rühle, *J. Am. Ceram. Soc.*, 1982, **65**, 642.
55 G. Skandan, H. Hahn, M. Roddy and W. R. Cannon, *J. Am. Ceram. Soc.*, 1994, **77**, 1706.
56 S. C. Moon, M. Fijino, H. Yamashita and M. Anpo, *J. Phys. Chem. B*, 1997, **101**, 369.
57 P. Scherrer, *Nachr. Ges. Wiss. Göttingen*, 1918, 96.
58 H. P. Klug and L. E. Alexander, *X-Ray Diffraction Procedures for Polycristalline and Amorphous Materials*, J. Wiley & Sons, New York, 1974.
59 *Gmelins Handbuch der anorganischen Chemie*, Verlag Chemie, Weinheim, 1973, Band 42 Zr.
60 R. Suyama, T. Asida and S. Kume, *J. Am. Ceram. Soc.*, 1985, **68**, 314.
61 M. Shoyama, N. Matsumoto, T. Hashimoto, H. Nasu and K. Kamiya, *J. Mater. Sci.*, 1998, **33**, 4821.